Hindawi Publishing Corporation
Advances in Materials Science and Engineering
Volume 2013, Article ID 823594, 7 pages
http://dx.doi.org/10.1155/2013/823594

Research Article

Characteristics Analysis and Testing of SMA Spring Actuator

Jianzuo Ma,[1] Haolei Huang,[1] and Jin Huang[2]

[1] *College of Mechanical Engineering, Chongqing Industry Polytechnic College, Chongqing 401120, China*
[2] *The Key Laboratory of Manufacture and Test Techniques for Automobile Parts, Chongqing University of Technology, Chongqing 400054, China*

Correspondence should be addressed to Jin Huang; jhuangcq@163.com

Received 19 July 2013; Accepted 8 September 2013

Academic Editor: Xing Chen

The biasing form two-way shape memory alloy (SMA) actuator composed of SMA spring and steel spring is analyzed. Based on the force equilibrium equation, the relationship between load capacity of SMA spring and geometric parameters is established. In order to obtain the characteristics of SMA spring actuator, the output force and output displacement of SMA spring under different temperatures are analyzed by the theoretical model and the experimental method. Based on the shape memory effect of SMA, the relationship of the SMA spring actuator's output displacement with the temperature, the stress and strain, the material parameters, and the size parameters is established. The results indicate that the trend of theoretical results is basically consistent with the experimental data. The output displacement of SMA spring actuator is increased with the increasing temperature.

1. Introduction

Shape memory alloy (SMA) is known as a kind of new intelligent material. SMA may undergo mechanical shape changes at relatively low temperatures, retain them until heated, and then come back to the initial shape [1, 2]. The outstanding quality characteristics of SMA are shape memory effect (SME) and super elasticity (SE) [3]. The shape memory effect, which allows the deformed material to recover a memorized shape when heated above the transformation temperature, can be exploited effectively in microrobots, automobile, automatic adjustment devices, aerospace, home appliances and daily necessities, [4–8] and so on.

An actuator based on these materials is made up of an SMA element that works against a contrasting element (a weight or other constant force, a conventional spring, or a second SMA element). At low temperature, the contrasting element overcomes the resistance of the easily deformable SMA element. The actuator is activated by heating the SMA element above the transformation temperature. The resulting increase in stiffness enables the SMA element to overcome the resistance of the contrast, thus generating useful displacements and producing mechanical work [3, 9–11].

In this paper, we present the biasing form SMA actuator, which is able to generate displacement and force. Based on the force equilibrium equation, the output force and output displacement of SMA spring under different temperatures are analyzed by the theoretical model and the experimental method. Based on the shape memory effect of SMA, the relationship of the SMA spring actuator's output displacement with the temperature, the stress and strain, the material parameters, and the size parameters is established. The output displacement of SMA spring actuator is increased with the increasing temperature.

2. Properties of SMA

The most commonly used SMA elements for actuators are helical springs, which for this form produce a large displacement. The force that a spring of any material produces at a given deflection depends linearly on the shear modulus of the material. SMAs exhibit a large temperature dependence on the material shear modulus. The relationship between shear modulus and temperature for SMAs is given by

$$G = \begin{cases} G_M & \text{when } T < M_f \text{ and } T < A_s, \\ G(\gamma, T) & \text{when } M_f \le T \le A_f, \\ G_A & \text{when } T > A_f \text{ and } T > M_s, \end{cases} \quad (1)$$

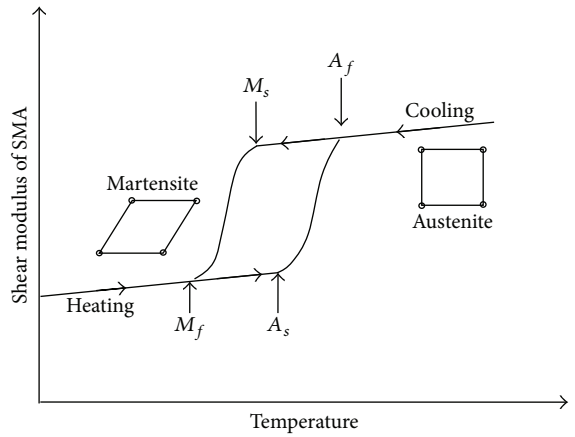

Figure 1: Transformation temperatures of martensite and austenite.

where G is the shear modulus of SMAs. T is temperature and M_s, M_f, A_s, and A_f are the start and finish transformation temperatures of martensite and austenite, respectively, as shown in Figure 1. G_M and G_A are the shear moduli of martensite and austenite, respectively. When $M_f \le T \le A_f$, in absence of stress, shear modulus of SMAs can be expressed approximately as

$$G(T) = G_M + \frac{G_A - G_M}{2}\left[1 + \sin\phi\left(T - T_m\right)\right]. \quad (2)$$

In the process of heating, $T_m = (A_s + A_f)/2$, $\phi = \pi/(A_f - A_s)$; in the process of cooling, $T_m = (M_s + M_f)/2$, $\phi = \pi/(M_s - M_f)$.

When the SMA wire is heated or cooled, the heat balance equation is

$$\rho_1 cV\frac{\mathrm{d}T}{\mathrm{d}t} = -hA\left(T - T_f\right), \quad (3)$$

where ρ_1 is the mass density of SMA, c is the specific heat, V is the volume of SMA exposed in air, t is the time, h is the heat exchange coefficient, A is the superficial area of SMA, and T_f is the temperature of airflow.

If $T = T_0$, when $t = 0$, the temperature variation of SMA wire with time is

$$T = \left(T_0 - T_f\right)\mathrm{e}^{-t/\varphi} + T_f, \quad (4)$$

where T_0 is the initial temperature and φ is the time constant of SMA wire, $\varphi = \rho_1 cV/hA$.

If the material and structural parameters of SMA have been determined, the time constant is inversely proportional to the heat exchange coefficient. Under three different heat exchange coefficients, the temperature variation of SMA wire with the around airflow temperature is shown in Figure 2. As shown in Figure 2, in a different heat exchange coefficient, the temperature of SMA wire changes faster when the time constant is smaller and the lag of time is shorter. When the time constant is less than 2.5, the lag time is less than 2 seconds.

3. Operational Principle of SMA Actuator

The SMA drive element uses the properties of low yield stress at martensitic state and returns to the high yield stress at austenite phase state when heated. Thus, the action form of a single SMA part is one-way. To obtain two-way characteristics of SMA elements, the structures of differential form and biasing from are used commonly. The differential form uses two or more SMA elements to obtain the two-way characteristics. The biasing form combines the one-way SMA with other parts to obtain two-way characteristics, shown in Figure 3, with the SMA helical spring working against a conventional steel spring (referred here as the "biasing" spring). At low temperatures, the steel spring is able to completely deflect the SMA spring to its compressed length. When increasing the temperature of the SMA spring, it expands, compressing the steel spring and moving the push rod.

4. Property Analysis of SMA Spring

Relative to the free length of the spring, the SMA spring provides a large action stroke, shown in Figure 4.

The expression for shear stress in an SMA spring is described as

$$\tau = \kappa\frac{8FD}{\pi d^3} = \kappa\frac{8FC}{\pi d^2}, \quad (5)$$

where the axial load is F, D is the average diameter of the spring, d represents the wire diameter, C is the spring index, $C = D/d$, and κ is known as the Wahl correction factor applied:

$$\kappa = \frac{4C - 1}{4C - 4} + \frac{0.615}{C}. \quad (6)$$

Shear stress τ has a relationship with shear strain γ which is

$$\tau = G \cdot \gamma. \quad (7)$$

The stretch of spring under the load F is

$$\delta = \frac{8FD^3 n}{d^4 G}, \quad (8)$$

where n is the number of turns in the spring.

The relationship between compressed length δ and shear strain γ for SMA spring is given by

$$\delta = \frac{n\pi D^2}{d}\gamma. \quad (9)$$

The wire diameter for the actuator can be obtained from (5) for acceptable values of C ranging from 3 to 12:

$$d = \sqrt{\kappa\frac{8FC}{\pi\tau}}. \quad (10)$$

The number of turns in the spring can be obtained from (9):

$$n = \frac{\Delta\delta d}{\pi\Delta\gamma D^2}, \quad (11)$$

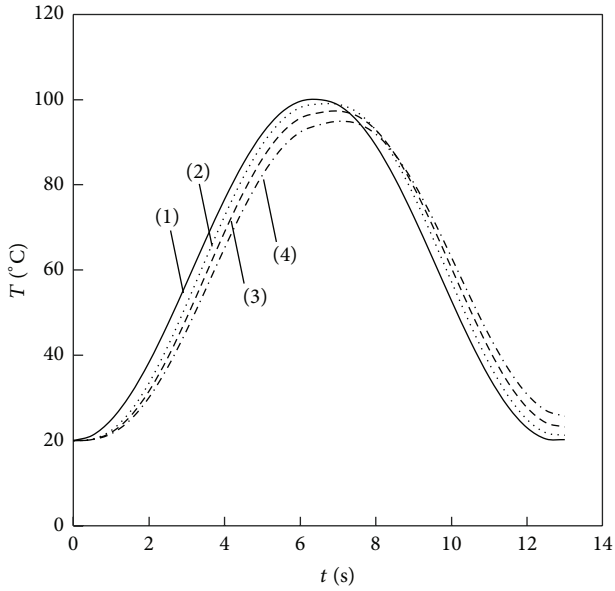

(1) The around airflow temperature
(2) The temperature of SMA when the time constant is 1.5
(3) The temperature of SMA when the time constant is 2.0
(4) The temperature of SMA when the time constant is 2.5

Figure 2: The temperature variation of SMA wire with the around airflow temperature under three different heat exchange coefficients.

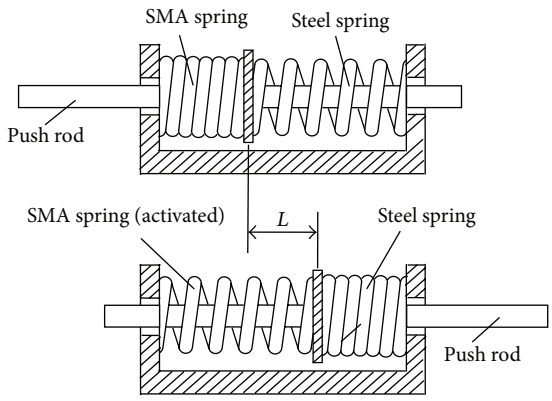

Figure 3: The operational principle of the SMA actuator.

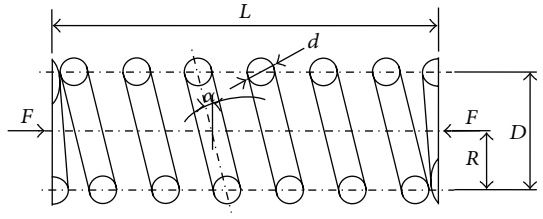

Figure 4: A compression helical SMA spring.

where $\Delta\delta$ represents the stroke of the actuator and $\Delta\gamma$ is the strain difference at high and low temperatures:

$$\Delta\gamma = \gamma_L - \gamma_H. \tag{12}$$

4.1. The Output Force of SMA Spring under Different Temperatures. The experimental system for the output force of SMA spring versus temperature under the constraint of displacement is shown in Figure 5 and the experimental device is shown in Figure 6.

As shown in (8), when $M_f \le T \le A_f$, the axial load at temperature T can be expressed as

$$F(T) = \frac{\delta(T) G(T)}{\delta_L G_L} F_L. \tag{13}$$

The axial load at low temperature is expressed as

$$F_L = \frac{d^4 G_L}{8D^3 n} \delta_L. \tag{14}$$

When the axial displacement of SMA spring is restricted, the compressed length of SMA spring is kept as

$$\delta(T) = \delta_L. \tag{15}$$

When $M_f \le T \le A_f$, the output force at temperature T can be obtained from (13), (14), and (15) as

$$F(T) = \frac{G(T) d^4}{8D^3 n} \delta_L. \tag{16}$$

In this study, Ti-49.8at.%Ni SMA spring is used, shown in Figure 7; its start and finish temperatures of the martensitic and austenitic phase transformation are $M_s = 78^\circ$C, $M_f = 50^\circ$C, $A_s = 74^\circ$C, and $A_f = 95^\circ$C, respectively. The shear

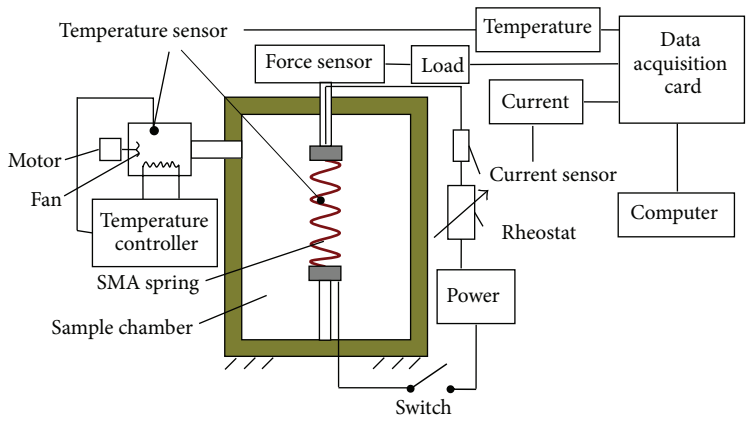

Figure 5: The experimental system for output force.

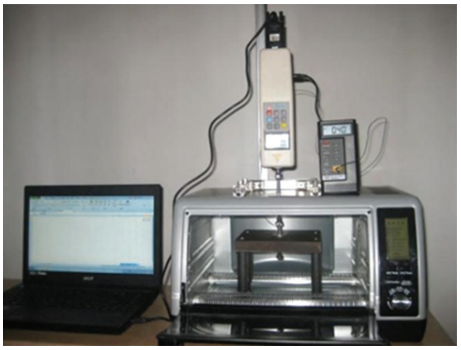

Figure 6: The experimental device for output force.

Figure 7: SMA spring sample.

moduli of martensite and austenite are $G_M = 7.5$ GPa and $G_A = 25$ GPa, respectively. The wire diameter of SMA spring is $d = 1$ mm, the angle of inclination is $\alpha = 6^\circ$, the diameter of SMA spring is $D = 8.6$ mm, and the number of turns is $n = 7$. When $\delta = 15$ mm, the theoretical and the experimental results of the relationship between the output force and temperatures of SMA spring are shown in Figure 8. The trend of theoretical results is basically consistent with the experimental data. The output force is increased with the rising of temperature.

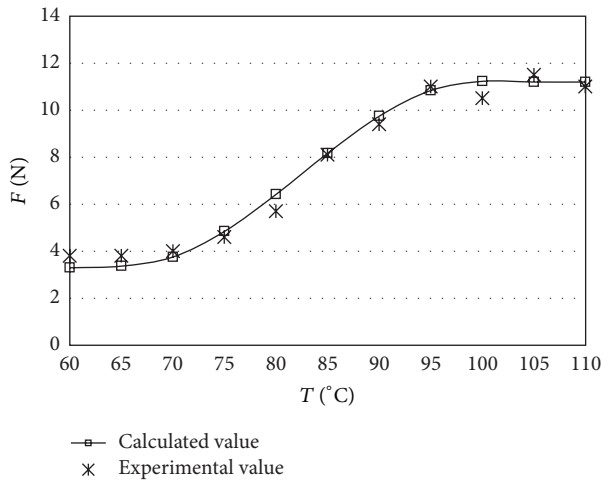

Figure 8: Output force versus temperature under the constraint of displacement.

4.2. The Output Displacement of SMA Spring under Different Temperatures. The experimental system for output displacement of SMA spring under different temperatures is shown in Figure 9 and the experimental device is shown in Figure 10.

As shown in (9), the compressed length can be expressed as

$$\delta = \frac{\pi D^2 n \gamma}{d}. \tag{17}$$

When $M_f \le T \le A_f$, shear strain γ is

$$\gamma = \frac{G_L \gamma_{\max}}{G}. \tag{18}$$

The output displacement can be obtained from (17) and (18) as

$$\Delta\delta = \frac{\pi D^2 n}{d}\left(1 - \frac{G_L}{G}\right)\gamma_{\max}. \tag{19}$$

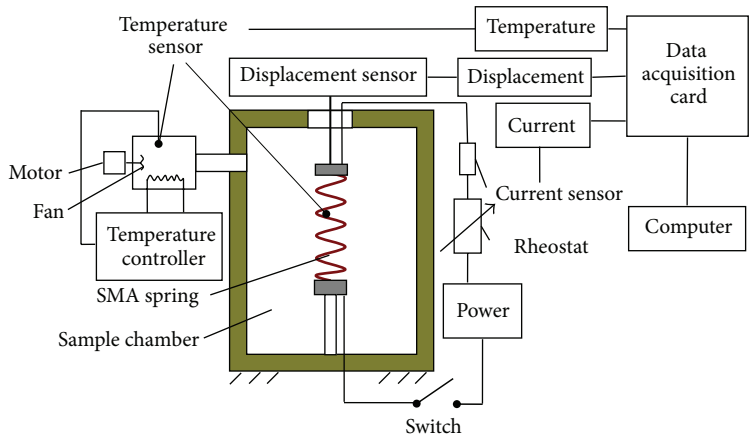

Figure 9: The experimental system for output displacement.

Figure 10: The experimental device for output displacement.

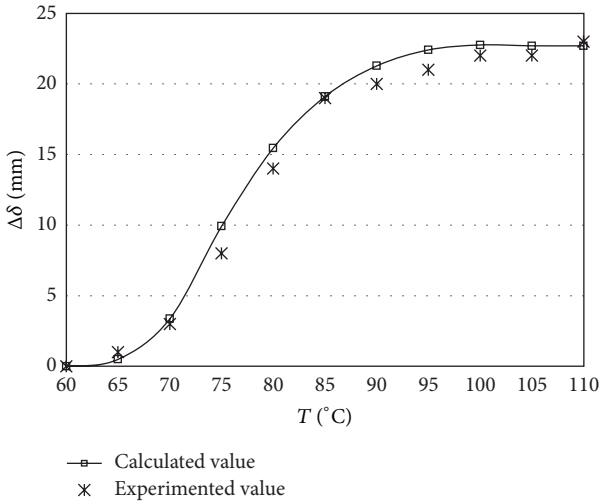

Figure 11: The output displacement of SMA spring versus temperature under constant load.

The typical SMA spring sample is shown in Figure 7; when the maximum shear strain is $\gamma_{\max} = 2\%$, the theoretical and the experimental results of the relationship between the output displacement and temperatures of SMA spring are shown in Figure 11. The trend of theoretical results is basically consistent with the experimental data. The output displacement is increased with the rise of temperature.

5. Analysis of SMA Actuator

The scheme of the proposed actuator with an SMA spring and conventional steel against spring is illustrated in Figure 3, where at low temperature the SMA spring will be compressed and when heated will extend with a pushing actuation. For the SMA actuator in Figure 3, the axial load of SMA spring F has the relationship with the compressed length of SMA spring δ as follows:

$$\frac{F(T)}{\delta(T)G(T)} = \frac{F_L}{\delta_L G_L},$$
$$F(T) = F_L + \frac{F_H - F_L}{\Delta\delta} S(T), \tag{20}$$

where $F(T)$, $\delta(T)$, and $G(T)$ are the axial load, compressed length, and shear modulus of SMA spring at temperature T, respectively; F_L, δ_L, and G_L are the axial load, compressed length, and shear modulus of SMA spring at low temperature, respectively; F_H is the axial load at high temperature; and $S(T)$ is the output displacement of SMA spring actuator:

$$S(T) = \delta_L - \delta(T). \tag{21}$$

The output displacement of SMA spring actuator can be obtained from (1), (2), (9), (20), and (21)

$$S(T) = \frac{(G(T) - G_L)\gamma_L}{(d/n\pi D^2)G(T) + ((F_H - F_L)/\Delta\delta F_L)G(T)\gamma_L}. \tag{22}$$

The experimental system for output displacement of SMA actuator under different temperatures is shown in Figure 12. The SMA helical spring works against a conventional steel spring to obtain the two-way SMA actuator. The typical SMA spring sample is shown in Figure 7. The stroke of the actuator is $\Delta\delta = 10$ mm. The effect of temperature on the output displacement of SMA spring actuator is analyzed by

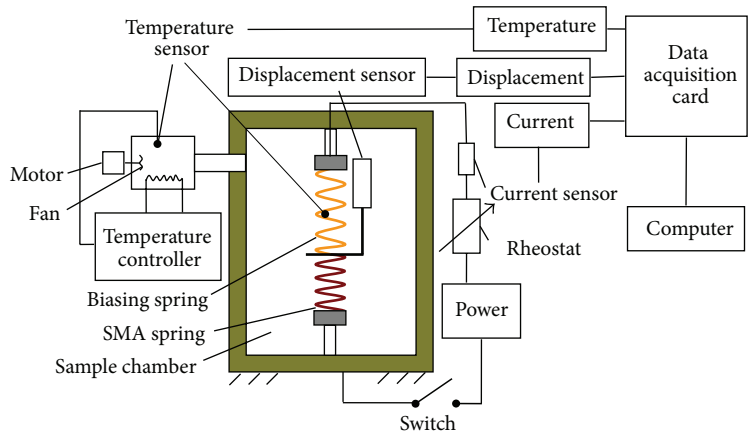

Figure 12: The experimental system for output displacement of SMA actuator versus temperature.

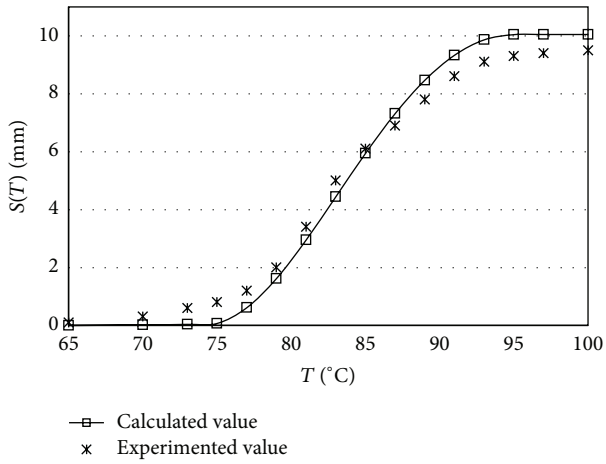

Figure 13: The output displacement versus temperature.

the theoretical model and the experimental method, shown in Figure 13. The axial loads of SMA spring at low and high temperatures are $F_L = 10\,\text{N}$ and $F_H = 30\,\text{N}$, respectively. The low temperature shear strain is $\gamma_L = 1.5\%$. As shown in Figure 13, the output displacement of SMA spring actuator is increased with the increasing temperature.

6. Conclusions

The characteristics and test method of SMA spring and SMA actuator are analyzed in this paper. The output force and output displacement equations of SMA spring are derived. The output force and output displacement are increased with the rise of temperature. The relationship of the SMA spring actuator's output displacement with the temperature is investigated theoretically and experimentally. With the increase of the temperature acting on SMA actuator, the output displacement of SMA spring actuator is increased proportionally.

Acknowledgments

This work was supported by the National Natural Science Foundation of China (51175532, 11272368) and by the Natural Science Foundation Project of CQ CSTC (Key Project CSTC, 2011BA4028).

References

[1] C. Yu, G. Kang, D. Song, and Q. Kan, "Micromechanical constitutive model considering plasticity for super-elastic NiTi shape memory alloy," *Computational Materials Science*, vol. 56, pp. 1–5, 2012.

[2] S. Huang, M. Leary, T. Ataalla, K. Probst, and A. Subic, "Optimisation of Ni-Ti shape memory alloy response time by transient heat transfer analysis," *Materials & Design*, vol. 35, pp. 655–663, 2012.

[3] G. Scirè Mammano and E. Dragoni, "Increasing stroke and output force of linear shape memory actuators by elastic compensation," *Mechatronics*, vol. 21, no. 3, pp. 570–580, 2011.

[4] A. Hadi, A. Yousefi-Koma, M. Elahinia, M. M. Moghaddam, and A. Ghazavi, "A shape memory alloy spring-based actuator with stiffness and position controllability," *Proceedings of the Institution of Mechanical Engineers, Part I: Journal of Systems and Control Engineering*, vol. 225, no. 7, pp. 902–917, 2011.

[5] B. Kim, S. Lee, J. H. Park, and J.-O. Park, "Design and fabrication of a locomotive mechanism for capsule-type endoscopes using shape memory alloys (SMAs)," *IEEE/ASME Transactions on Mechatronics*, vol. 10, no. 1, pp. 77–86, 2005.

[6] S. Langbein and A. Czechowicz, "Adaptive resetting of SMA actuators," *Journal of Intelligent Material Systems and Structures*, vol. 23, no. 2, pp. 127–134, 2012.

[7] B. Kim, M. G. Lee, Y. P. Lee, Y. Kim, and G. Lee, "An earthworm-like micro robot using shape memory alloy actuator," *Sensors and Actuators A*, vol. 125, no. 2, pp. 429–437, 2006.

[8] T. Georges, V. Brailovski, and P. Terriault, "Characterization and design of antagonistic shape memory alloy actuators," *Smart Materials and Structures*, vol. 21, no. 3, Article ID 035010, 2012.

[9] R. Lahoz and J. A. Puértolas, "Training and two-way shape memory in NiTi alloys: influence on thermal parameters," *Journal of Alloys and Compounds*, vol. 381, no. 1-2, pp. 130–136, 2004.

[10] M. Mertmann and G. Vergani, "Design and application of shape memory actuators," *European Physical Journal*, vol. 158, no. 1, pp. 221–230, 2008.

[11] C. Mavroidis, "Development of advanced actuators using shape memory alloys and electrorheological fluids," *Research in Nondestructive Evaluation*, vol. 14, no. 1, pp. 1–32, 2002.